nature nanotechnology

Article

https://doi.org/10.1038/s41565-023-01316-3

Imaging solid–electrolyte interphase dynamics using operando reflection interference microscopy

In the format provided by the authors and unedited

SUPPLEMENTARY INFORMATION

Imaging Solid-Electrolyte-Interphase Dynamics Using Operando Reflection Interference Microscopy

Contents:

Section 1. Materials and setup configuration

1. Materials.

The copper (Cu) film substrate was fabricated via thermal evaporation with a thickness around 35 nm on a 150 μm-thick glass slide (refractive index: 1.5). Lithium (Li) mental foil was purchased from Sigma-Aldrich and the surface was cleaned by doctor blade before using. $LiPF_6$ and propylene carbonate (PC) at battery grade were purchased from BASF Corporation and used without further purification. The electrolyte of 1.0 M $LiPF_6$ in PC was prepared inside an argon-filled glovebox where the oxygen and moisture content were less than 0.5 ppm. The H_2O content in this electrolyte was about 13 ppm, measured by Karl Fisher titration. The electrolyte with 50 ppm H_2O as an additive was prepared by adding additional 50 ppm deionized water into the above 1.0 M $LiPF_6$/PC electrolyte and used after storage of 2 days to allow the reaction of $LiPF_6$ and water to reach equilibrium. The Cu substrate was immersed in 0.1 M HCl to remove the Cu oxide layer before the reaction. Then the electrode surface was cleaned with deionized water and acetone sequentially to remove the HCl residues.

2. Cell preparation

A three-electrode system was used in this study, where the Cu film coated substrate worked as the working electrode and Li metal worked as the counter and reference electrodes, respectively. A hollow cylindrical reservoir with the diameter of 2 cm and height of 1.2 cm was placed and sealed on the Cu substrate using epoxy glue. Two types of electrolytes were used in our tests, 1.0 M $LiPF_6$ in PC with 50 ppm H_2O as additive was used to study the H_2O effect, and the same electrolyte but without additional water was used as a control electrolyte.

3. Optical imaging and electrochemical condition synchronization

To ensure that the entire SEI formation process can be completely recorded, optical imaging was recorded in advance and then the electrochemical conditions were applied to trigger the evolution of the

stratified SEI components. By using a Labview card (National Instruments USB-6009), all the optical signals and images from the camera, and the current and potential signals from electrochemical workstation can be accurately synchronized in real-time. Generally, the data acquisition card can collect the electrochemical signal data stream and the charge-coupled device (CCD) imaging pulse signal at the same time. Then with a MATLAB code, we can precisely find the specific time when the electrochemical condition is implemented and associate each frame of image with its corresponding practical electrochemical information. The synchronization between the optical images and the electrochemical information enables the analysis of real time electrochemical reaction dynamics on the electrode surface and the synchronized imaging information is essential for further structural stratified SEI thickness and localized distribution analysis.

4. Electrochemical test condition conditions

To investigate the SEI evolution dynamics on the substrate surface and the main composition difference during different cycles, a cyclic voltammetry (CV) mode was performed with CHI660E (CH Instrument Ins.), starting from 2.3 V to 0.1 V vs. Li/Li^+. For both electrolytes, 1.0 M $LiPF_6$ in PC with 50 ppm H_2O additive and 1.0 M $LiPF_6$ in PC without additional water as control, nine scan cycles were conducted to analyze the dynamic changes of SEI formation in different cycles. Since the CV curve only exhibited obvious difference in the first cycle (the LiF-rich layer mainly formed within the first cycle), we showed the first three cycles scanning data (**Figs. 1b-e**, **Supplementary Fig. 1** and **2**) in the main text. A constant current mode (0.1 mA cm^{-2}) was also performed to further certify the phenomenon that we observed in CV mode and to investigate the correlation between the LiF-rich and organic SEI layers and the influence of the formed SEIs on the following Li nucleation process.

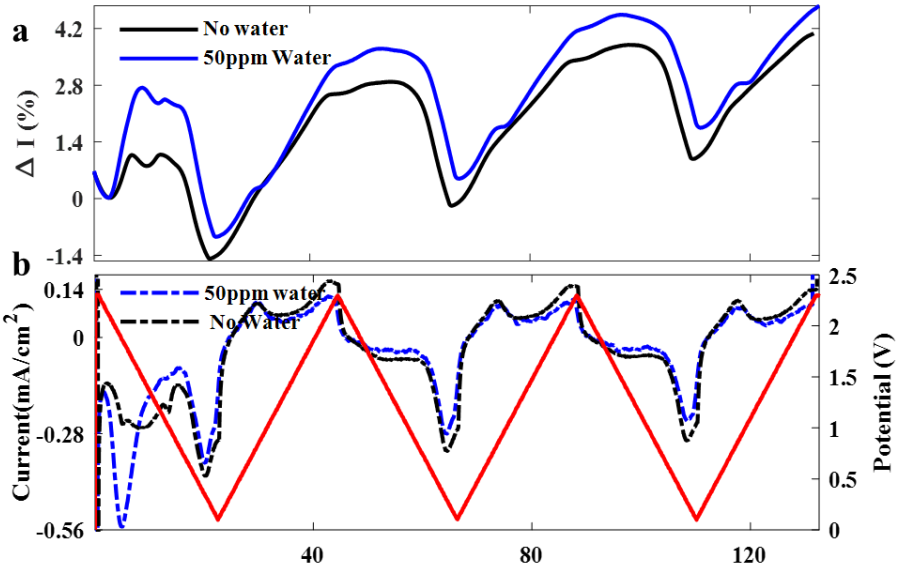

Supplementary Fig. 1 | *In-situ* characterization of the dynamic formation of SEI on Cu surface in different electrolytes. a, The optical response during the first three cycles of CV scans. **b,** The first three cycles of CV scans (red curve) and the corresponding current response.

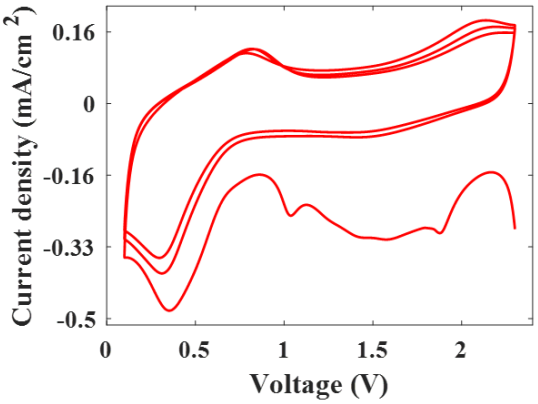

Supplementary Fig. 2 | The first three cycles CV curve, when the electrolyte was in absence of water additive.

Section 2. Verification and calibration of RIM

1. Verification of RIM.

When the light is reflected from different surfaces of a thin film, the interference will happen, and a phase difference will be introduced to influence the detected optical reflectance intensity. The observed total reflection intensity I is described by the superposition of two reflected beams:

$$I = I_1 + I_2 + 2\sqrt{I_1 I_2}\cos\left[\frac{2\pi}{\lambda} * 2\boldsymbol{t}n + \delta\right]$$

Where I_1 and I_2 represent the reflected intensity from the top and bottom surfaces of the thin film, λ is the wavelength of the incident light, $\boldsymbol{t}$ is the thickness of the film, and n is the refractive index of the thin film. Here, a constant phase $\delta = \pi$ is taken into account, because an additional phase shift will happen at the medium-object interface if the object has a higher refractive index than the medium, which is electrolyte in our case. In another word, when the thin layer has a refractive index smaller than the electrolyte, no additional phase shift occurs, and the constructive interference happens and therefore the reflected optical intensity will increase as the thickness of the thin film increases (the period phenomenon was not considered in our case since the thickness of stratified SEIs are usually tens of nanometers). On the other hand, when the light reflects from an interface that having an index of refractive greater than that of the electrolyte, a 180° phase delay occurs which leads to destructive interference and the reflected intensity will decrease as the thickness of the thin film increases. More importantly, the interference induced optical reflectance response is highly dependent on the refractive index of the specific species, providing possible ways to recognize different components and do quantitative analysis. Theoretically, by detecting the reflected intensity change, we can recognize some characteristics of the component that is deposited on the substrate and once the refractive index is determined, the precise quantitative analysis can be realized.

We use the poly(methyl methacrylate) (PMMA) thin film, which has a known refractive index (Refractive index RI = 1.49) to experimentally demonstrate the feasibility of the interference method and further clarify the schematic of our RIM. The very thin layer of PMMA was spin-coated on the Cu substrate (495PMMA A resists, 4% in Anisole, spin speed: 1800 rpm) and the RIM was used to image the PMMA film's morphology (**Supplementary Fig. 3a**). There are two gray interference stripes (pointed by the black arrows, one is in the center, and the other one is on the edge) shown in the **Supplementary Fig. 3a**, which are induced by the interference effect generated from the PMMA thickness variations.

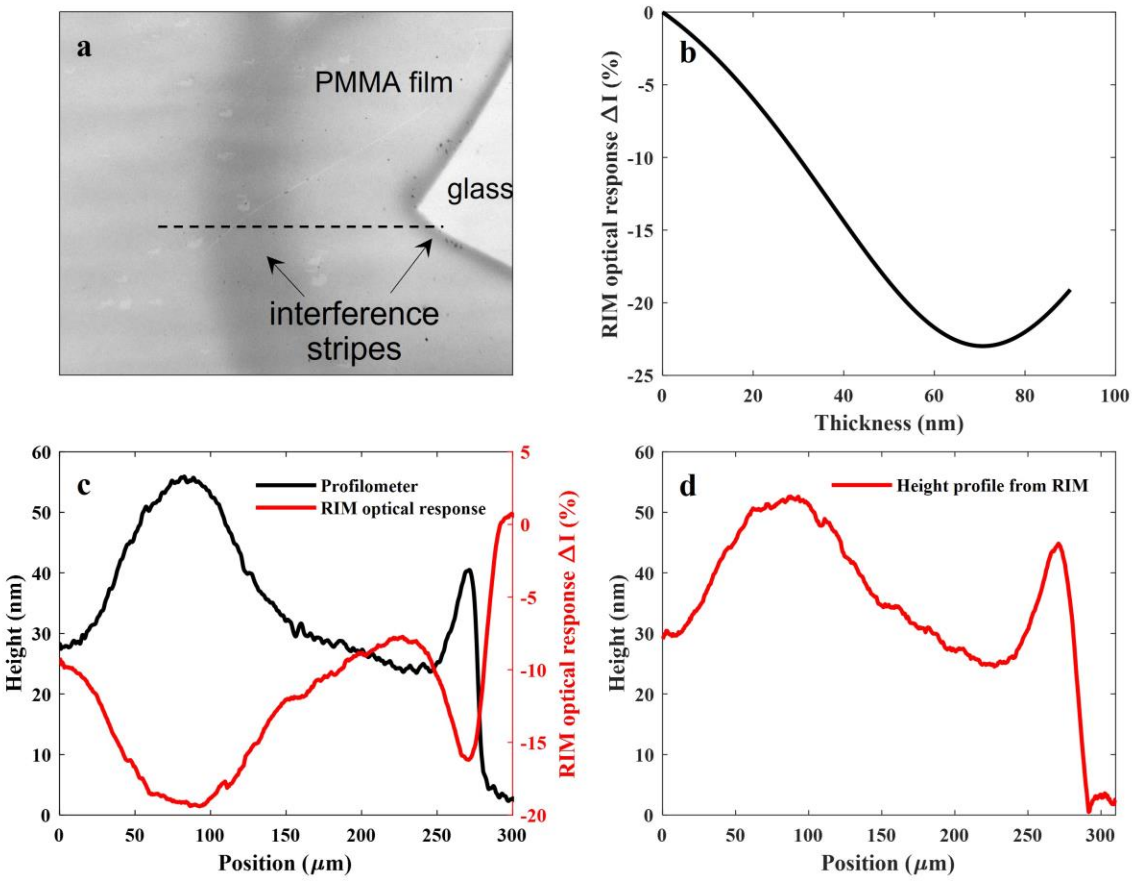

Supplementary Fig. 3 | Verification of the RIM through profilometer. a, Optical image of PMMA coated Cu substrate. **b,** Theoretical simulation of the optical reflectance variations according to thickness change of thin PMMA film. **c,** Thickness measured by profilometer and corresponding optical intensity response. **d,** Thickness profile calculated from the RIM optical responses.

To verify the RIM, we compare the RIM results with the profilometer. We have measured the thickness along the black dashed line in **Supplementary Fig. 3a** using the profilometer. The profile is shown in **Supplementary Fig. 3c** (black curve). We have also plotted the optical response from RIM together with the profilometer profile in **Supplementary Fig. 3c** (red curve). Using the refractive index of the PMMA, we can accurately calculate the conversion curve (**Supplementary Fig. 3b**), and convert the optical response obtained by the RIM to the thickness (**Supplementary Fig. 3d**). The obtained RIM profile (**Supplementary Fig. 3d**) shows good correlation with the profilometer result (**Supplementary Fig. 3c** black curve).

Supplementary Fig. 4 shows the correlation between the RIM and the profilometer results and the correlation is very close to 1 which indicates the accuracy of the RIM. In addition, RIM could provide a thickness map easily compared with profilometer.

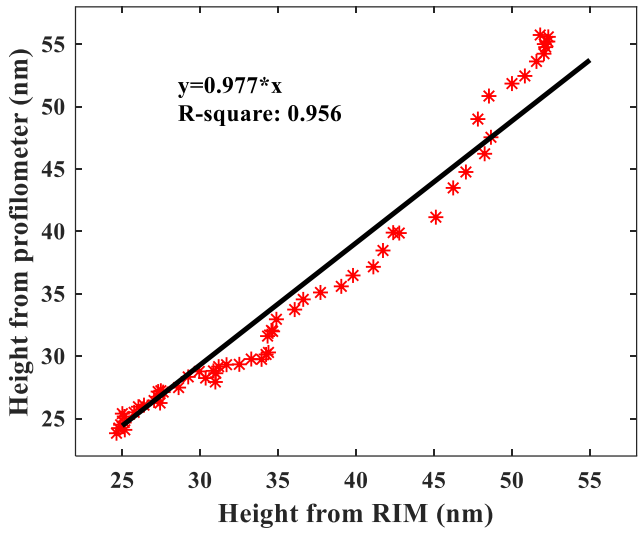

Supplementary Fig. 4 | Correlation between the thickness measured by RIM and by profilometer.

The monochromatic light source, such as laser or laser diode, can help obtain accurate interference optical response. However, the induced interference patterns and their drifts from the coherent light source will kill the small variations. Therefore, we balanced the monochromaticity and the stability of the light source and chose to use a bandpass filter on a broad band light source. The bandpass filter will allow a small range of wavelengths to pass through. Different wavelengths of light will have different interference and the overlap of these lights might disturb the total interference pattern. To minimize this effect, we intentionally chose a relatively narrow bandpass filter (Full width half maximum is ~ 10 nm). A bandpass filter with ~10 nm band width to filter the broadband light source. **Supplementary Fig. 5** shows the spectrum after passing the filter measured on the RIM setup. Since the wavelength range is much smaller than the wavelength, the effect to the interference pattern is minimized. To verify this hypothesis, we have calculated the conversion curves that can translate the RIM to thickness using a pure 600 nm light source vs. a light source that has been used in our experiment (spectrum is shown in **Supplementary Fig. 5**). The results are shown in the **Supplementary Fig. 6**. The difference is very small which demonstrates that the

light source we used will not disturb the interference. All the conversion curves we used in this work were calculated from the light source with the bandpass filter.

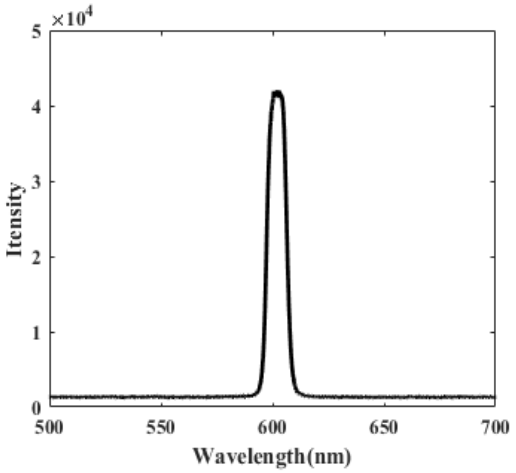

Supplementary Fig. 5 | Light source spectrum.

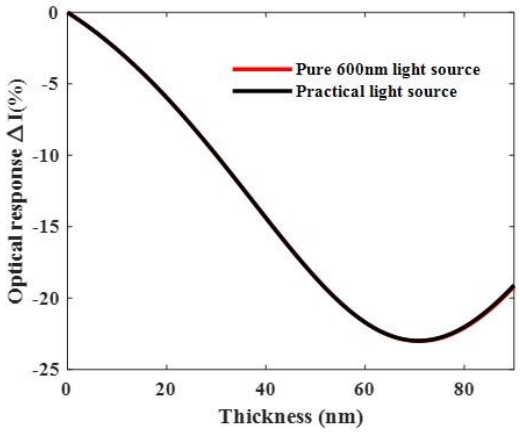

Supplementary Fig. 6 | Conversion curves with different light source.

2. Possible SEI components.

Due to the sensitivity of SEI components to different characterization methods, minor differences may occur when analyzing the chemical compositions of SEI. However, according to various reported results, most of the possible species of SEI can be summarized as inorganic components, including LiF (refractive index: 1.39), Li_2O (refractive index: 1.64), Li_2CO_3 (refractive index: 1.43), LiH (refractive index: 1.98),

LiOH (refractive index: 1.46), and organic components[1, 2, 3, 4, 5], such as Li semicarbonates and Li dicarbonates (when carbonate solvents are used). Considering the refractive index of the electrolyte is usually larger than 1.41[6, 7], only the LiF has a smaller refractive index than the surrounding electrolyte.

3. Calibrate the optical properties of SEI layer.

The accuracy of the RIM method has been verified with PMMA, therefore we next use it to obtain the optical properties (the refractive index) of SEI layer. The sample was prepared by negatively scanning the Cu substrate from 2.3 V to 1.4 V, and the electrode was held at 1.4 V for another 100 s. The electrode was covered by a PDMS to block the formation of SEI underneath the PDMS region. This will create a clear boundary between the bare Cu electrode and the LiF-rich proto-SEI layer. The substrate was cleaned with DMC solvent for three times before the RIM image was obtained in Ar. At the same time, we used the AFM to measure the thickness of the SEI layer. Since we know the SEI's thickness from the AFM measurement and the RIM optical response, we can calibrate the optical properties of this SEI layer using the interference calculation.

All AFM characterizations were conducted with Asylum Research MFP-3D Origin+ atomic force microscope (Oxford Instrument). Tapping mode was adopted to obtain surface morphology and roughness using OPUS 160AC silicon probe (MikroMasch, $f_0 = 300\ kHz, k = 26\ N\ m^{-1}$).

The SEI boundary was imaged by the RIM firstly, and the marker was made on the electrode surface to track the location (arrow in **Supplementary Fig. 7a**). After the RIM imaging, the exact location was found in the AFM system using the marker we created, and morphology imaging was performed using AFM. **Supplementary Fig. 7a** and **d** show the RIM image of the SEI boundary, and the corresponding AFM image. The black dashed rectangle shows the region of AFM mapping (**Supplementary Fig. 7d**) on the RIM image (**Supplementary Fig. 7a**). The AFM image clearly shows the boundary between the SEI layer and the bare Cu surface, implying that the deposition of the LiF-rich species will lead to a thickness increase on the right side of image. The relocation to the same area on the AFM setup is challenging which

leads to a limited calibration result. However, we did perform further analysis of the data that we collected.

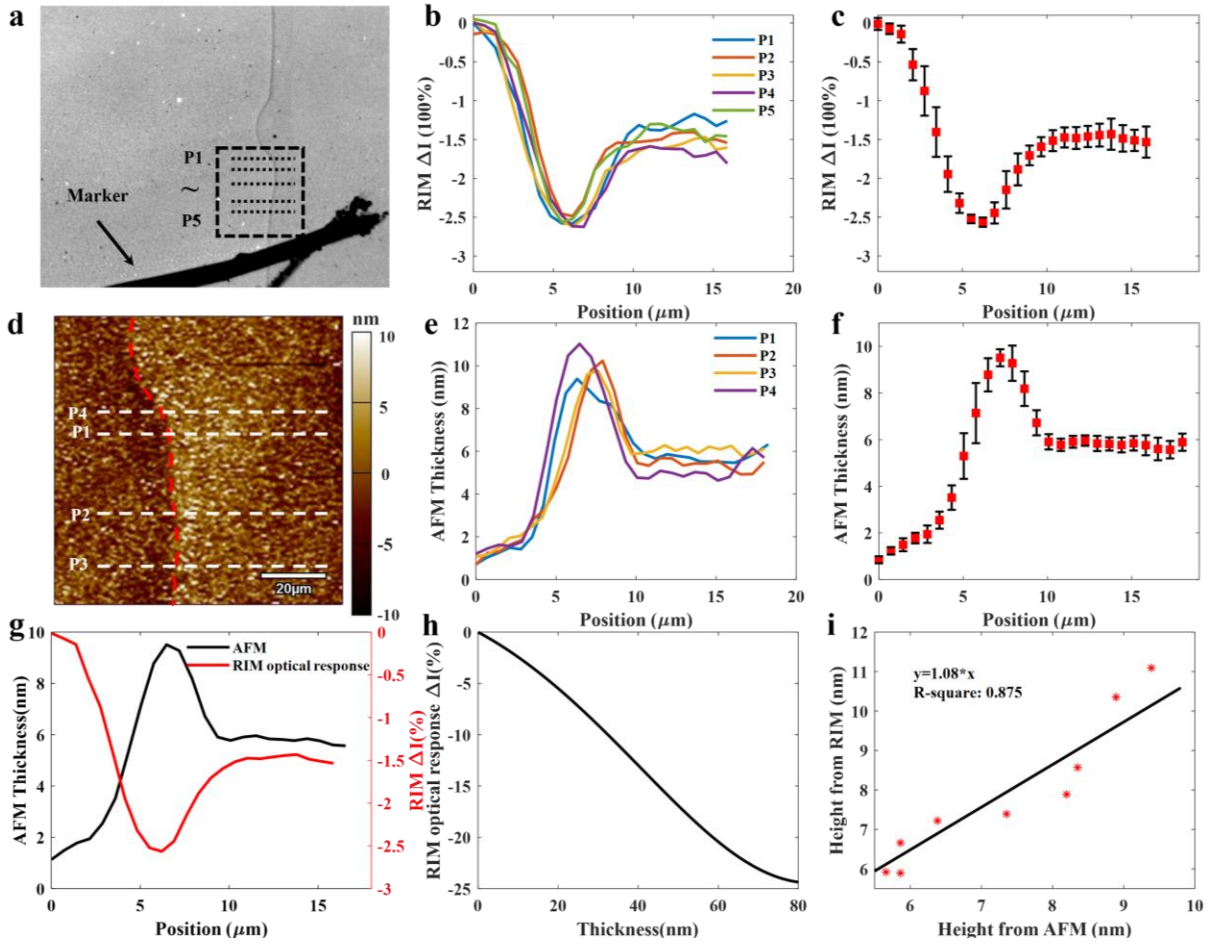

Supplementary Fig. 7 | Comparison between AFM and RIM measurement of LiF-rich layer. a, RIM image of LiF-rich species accumulated Cu substrate. **b**, RIM intensity profiles at different regions along the dash line in (**a**). **c**, The average and error bar plot of the RIM intensity response. The data are presented as mean ± SD (n=5). **d**, AFM image of LiF-rich species accumulated Cu substrate. **e**, Thickness profiles at different regions along the dash line in (**d**). **f**, The average and error bar plot of the AFM thickness profile. The data are presented as mean ± SD (n=4). **g,** AFM measured thickness and corresponding optical reflectance response. **h,** Theoretical simulation of the optical reflectance variations according to thickness change of proto-SEI layer. **i,** Correlation between the

Supplementary Fig. 7b shows the RIM response across the SEI step at different locations (labeled with dash line in **Supplementary Fig. 7a**) and the **Supplementary Fig. 7e** shows the step responses on AFM images at different locations. The average response from RIM and AFM are plotted in **Supplementary Fig. 7c** and **Supplementary Fig. 7f**, correspondingly. Considering it is difficult to find exact locations to match individual curves between the RIM and AFM, we plot the averaged RIM response and the AFM thickness

response together, as shown in **Supplementary Fig. 7g**, and use these two to calibrate the refractive index of LiF-rich SEI layer. By using the AFM thickness and the RIM signal, we can fit out the refractive index of the LiF-rich layer which is ~1.32. The corresponding conversion curve between the RIM signal to the thickness is shown in the **Supplementary Fig. 7h**. And the **Supplementary Fig. 7i** shows good correlation between the AFM thickness and the RIM result when we use the 1.32 as the refractive index. Therefore, using refractive index of 1.32 for LiF-rich SEI layer calculation is reasonable and accurate.

Section 3. Surface roughness measured by AFM

The surface roughness of clean Cu working electrode and electrode with accumulated LiF-rich species are measured by AFM to support the results shown in **Fig. 4h**. To image the surface roughness of LiF-rich SEI layer, we have used the AFM to map the surface morphology before and after the LiF-rich layer's formation. The LiF-rich SEI was prepared by negatively scanning from 2.3 V to 1.4 V, then holding at 1.4 V for 100 s. **Supplementary Fig. 8a** shows the morphology of the LiF-rich SEM layer. In addition, we randomly select a line across the imaging region and plot the corresponding profile in **Supplementary Fig. 8b**. A large height fluctuation is observed, and the roughness (standard deviation) is calculated ~ 1.1 nm, which is close to the roughness calculated by optical method (~ 0.95 nm in **Fig. 4h**). On the other hand, the bare Cu electrode shows a much smoother surface (**Supplementary Fig. 8c**), and the profile shown in **Supplementary Fig. 8d** also exhibits a much smaller roughness. The surface roughness is calculated ~ 0.6 nm.

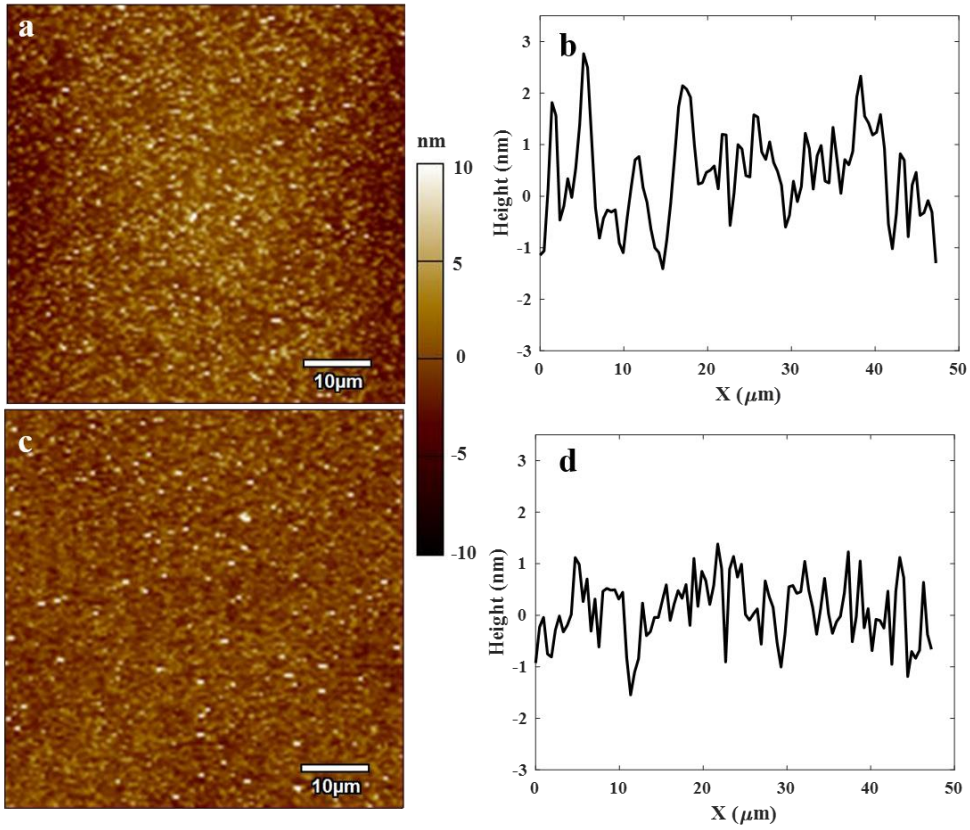

Supplementary Fig. 8 | AFM imaging of the bare substrate and the LiF-rich layer formed substrate surface. **a,** AFM imaging of LiF-rich SEI layer. **b,** Cross section profile of the LiF-rich layer. **c,** AFM imaging bare Cu. **d,** Random cross section profile of the Cu surface.

Section 4. Electric double layer formation at the electrode interface

When the EDL is formed on the electrode surface, there will be same amount of opposite charges accumulated on the metal electrode surface. This charge accumulation in the metal film will change charge density and therefore varies the permittivity of the very top layer of the metal electrode (**Supplementary Fig. 9**). It will lead to the reflectance change that can be measured by the RIM. Of course, EDL itself will not lead to a significant permittivity change. Instead, the signal comes from the opposite charges accumulated in the metal layer.

In our previous publication[8], we have also discussed and provided quantitative experimental results that match with the theory predictions. We have derived the theory starting with the Drude model, and we

showed that the reflectance from a conductive surface is a linear function of the surface charge density variations induced by applying potential to the electrode. This relation can be described with the equation shown below:

$$\Delta R(x, y, t) = -\beta \cdot \Delta\sigma(x, y, t) \qquad (1)$$

where

$$\beta = \frac{4n_i(n_i - n_m)}{(n_m + n_i)^3} \cdot \frac{\alpha}{2n_m e d_p} \qquad (2)$$

and

$$\alpha = e^2/\varepsilon_0 m_e 4\pi^2 f^2 \qquad (3)$$

In these equations, $n_m = n_r + in_i$ and the n_m, n_r, n_i, ΔR, $\Delta\sigma$, e, m_e, ε_0, and f are refractive index of metal, real part of metal refractive index, imaginary part of metal refractive index, reflectance change caused by the charge accumulation, surface charge density change in the metal film, electron charge, electron mass, vacuum permittivity, and frequency of the incident light. We can see the linear dependence between the accumulation of charge ($\Delta\sigma(x, y, t)$) with the reflectance map of RIM ($\Delta R(x, y, t)$) in equation (1). And our experimental results verified the theory prediction (see Fig. 2C and Fig. 3A[8]).

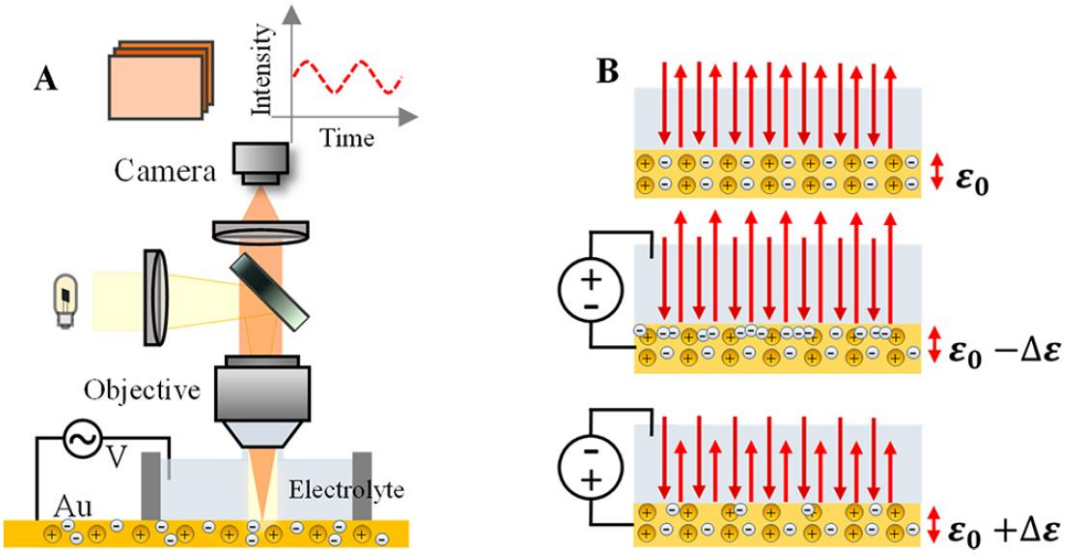

Supplementary Fig. 9 | Principle of using RIM to measure the charging effect generated by the formation of EDL. a, Experimental setup. **b,** The schematic drawing of charging effect on the metal permittivity and the reflection intensity of the light.

Section 5. SEI evolution processes

1. LiF-rich layer formation.

Supplementary Fig. 1 shows three cycles CV scan in electrolyte without and with 50 ppm water additive and the corresponding optical signals. In the first cycle of CV scan, a huge HF reduction peak was observed in **Fig. 1b, Supplementary Fig. 1b and Fig. 2**, indicating more HF is electrochemically reduced to LiF through equation (2). Correspondingly, comparing with the optical response in control electrolyte, we observe a larger optical signal which signifies more accumulation of the LiF-rich layer when additional water is added. This result confirms that the LiF-rich layer formed in part I is induced by water additive.

In addition, a holding potential experiment was performed to demonstrate the electrochemical reaction that happened during part I. To deposit the LiF-rich layer on the electrode surface, we did a CV scan from 2.3 V to 2.0 V, and then held at 2.0 V for 100 s but for the control experiment the potential was directly removed. The obtained optical signals shown in **Supplementary Fig. 10** indicates that compared with the

control experiment (blue curve in **Supplementary Fig. 10**), when holding potential at 2.0 V, the obtained optical signal (black curve in **Supplementary Fig. 10**) is obviously larger, demonstrating that more electrochemically reduced LiF-rich component is accumulated and further proving that during part I, the LiF-rich layer formation is the dominant process.

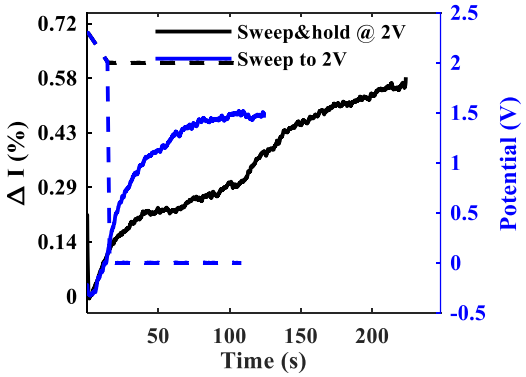

Supplementary Fig. 10 | Holding potential experiment to demonstrate the reaction that happens during part I.

Another holding potential experiment was carried out to further explain the potential window for LiF-rich SEI formation and prove that optical signal was indeed induced by electrochemical reactions. As shown in **Supplementary Fig. 11**, when we negatively polarize the electrode from 2.3 V, we will firstly observe an increasing optical signal which is related to the accumulation of LiF-rich SEI layer. As the potential becomes more negative, the electrical double layer starts to form. Holding potential at 1.0 V, where we believe neither LiF-rich SEI nor organic-rich SEI will accumulate at this potential, we find that the optical signal (marked with blue background) almost remains the same. This observation enhances our conclusion that during the potential window from 2.3 V to 1.3 V, what mainly occurs is the electrochemical reduction of HF and the accumulation of the produced LiF-rich components. In addition, this experiment also directly proves that the optical signal is sensitive to surface reactions, when there are no surface reactions there will be no obvious optical signal variation. Further certifying and highlighting the feasibility and stability of our method.

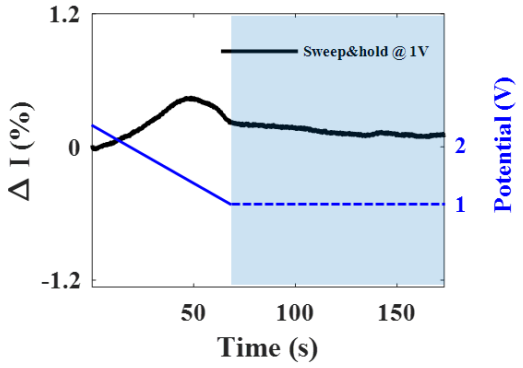

Supplementary Fig. 11 | Holding potential experiment demonstrating that the optical signal will remain constant when there is no SEIs accumulated on the electrode surface.

2. Partial oxidation of organic-rich layer.

To demonstrate the partially oxidization of organic-rich layer, another holding potential experiment was performed. The working electrode was firstly negatively polarized from 2.3 V to 0.1 V to deposit the SEIs on the substrate and then positively polarized to 1.8 V. After that, the electrode was then held at this cut-off potential for 100 s or directly removed the external potential as a control. During these processes, the electrode surface was continuously monitored, and the averaged optical signals were extracted and summarized in **Supplementary Fig. 12a**. In the control experiment, the original increasing optical signal stops immediately and become flat after removing the potential (blue curve in **Supplementary Fig. 12a**), because the electrochemical reaction stops and very small amount of components will keep releasing from the substrate. In comparison, when holding potential at 1.8 V, the optical signal continues to increase. Combining with the positive current shown in **Supplementary Fig. 12b** during the holding potential process (marked by blue background), we can easily conclude that when holding potential at 1.8 V, there is still electrochemical oxidization happening and releasing more organic components from the substrate. Therefore, a continuously increasing optical signal is observed (black curve in **Supplementary Fig. 12a**).

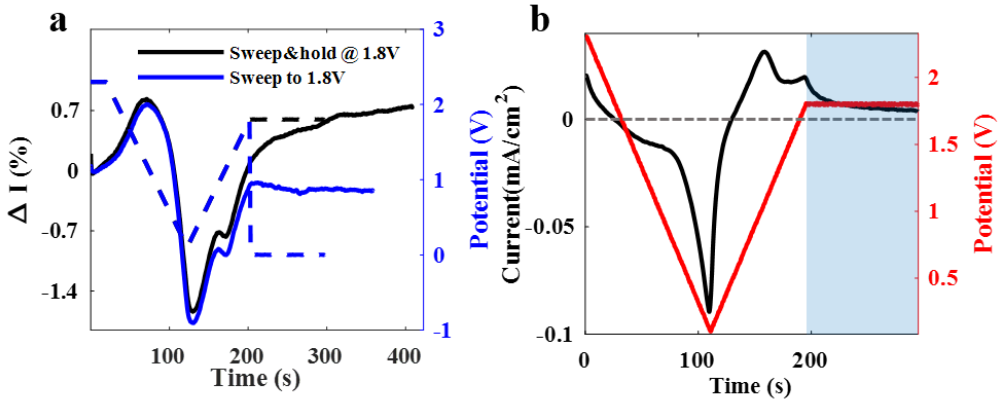

Supplementary Fig. 12 | Holding potential experiment to demonstrate the partially oxidization of organic components. a, The obtained optical signals when hold potential at 1.8 V (black curve) and directly remove the potential (blue curve). The corresponding dash line indicate the applied potential. **b,** The current response (black curve) during the holding potential experiment. The horizontal dash line marked the current density value of 0 and the blue background labeled the holding potential region.

Section 6. Converting reflectance to thickness

1. Optical signal to thickness information.

We use Winspall to simulate the conversion curves. Winspall is a software package to mainly help calculate the surface plasmon resonance response based on the Fresnel equations. The Fresnel equations describe the reflection and transmission of light when the incident happens on an interface between different optical media, making Winspall also proper for calculating the reflectivity response from multilayer system in our case. A dual-layer structure of the SEI is applied in our simulation since it confirms the already reported conclusions and satisfies the optical response in our experiments. The parameters we used for simulation are listed in **Supplementary Table 1**. For the inner LiF-rich layer, the refractive index is set as 1.32, which has been calibrated in **Section 2**. The parameter is smaller than 1.39 (pure LiF), one of the reasons is that the density of the species plays a critical role in determining the refractive index, and usually the density of the LiF produced by the electrochemical reaction is smaller than those formed by thermal evaporation method[9, 10]. In addition, the refractive index of LiF is decided to be 1.39 under stable conditions, but the newly formed LiF usually has a rather small refractive index value, which will increase as time

passes by and finally stabilizes at ~1.39[9]. Furthermore, other inorganic species will also influence the optical property of the generated layer. Once the refractive index of the media is determined, the detected reflectivity will change according to the thickness information of the media. **Supplementary Fig. 13a** describes how the reflectivity response changes along with the thickness change of the inorganic layer (inner LiF-rich layer) according to the simulation result. Utilizing this response curve, we can easily calculate the thickness information of the inorganic layer formed on the substrate surface from the detected related optical signal. The refractive index for the organic-rich layer is estimated as 1.46 with a small imaginary part. The optical response caused by the thickness change of the outer organic layer is simulated and plotted in **supplementary Fig. 13b**, which facilitates the thickness calculation of the organic-rich layer based on the detected optical signal. Another thing we should note is that when simulating the optical response with the organic-rich layer, the thickness of LiF-rich inner layer was fixed as a constant, which was rational since the LiF-rich and organic-rich SEIs were evolved at different potential windows. And considering the content of the LiF-rich layer is quite different for the electrolyte in absence or presence of H_2O additive, the thickness of the inner layer that used to simulate the relationship between organic layer and optical response will be adjusted accordingly to the specific situation for more accurate calculation.

Exact quantification using RIM is challenging because of the complicated compositions of the solid-electrolyte-interphase (SEI). The refractive index should be a combination that includes several reduction species which are difficult to measure. Besides, the refractive index is also related to the degree of looseness or denseness of the material accumulation, making it even harder to determine the exact refractive index. Therefore, what we calculate is the approximate thickness information of SEIs.

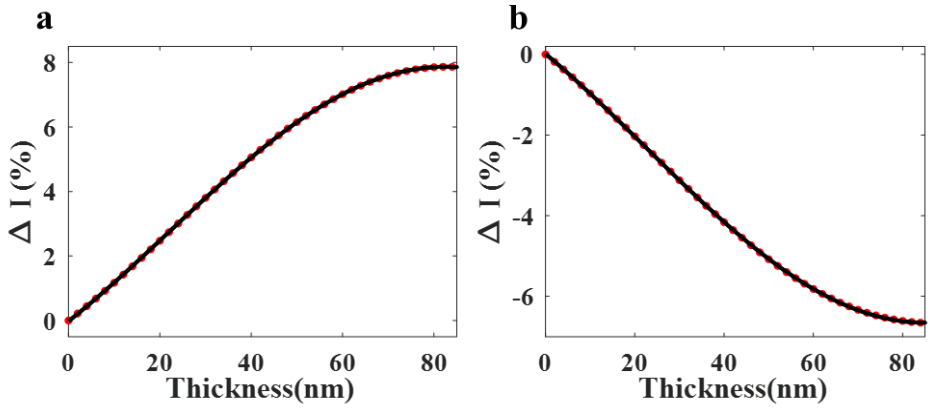

Supplementary Fig. 13 | Conversion curves for inner LiF-rich SEI layer and outer organic-rich SEI layer. a, Simulation between the reflectivity and the inner LiF-rich layer thickness. **b,** When an outer organic layer forms at the top of the LiF-rich layer.

Supplementary Table 1

Layer catalog	Thickness (nm)	Refractive index (n, k)
Bulk electrolyte	0	1.415
Organic-rich SEI	variable	1.46, 0.008
LiF-rich SEI	variable	1.32
Cu	30	0.49366, 2.9624
Glass substrate	0	1.51

2. Detection sensitivity of the in-operando RIM

To minimize the drift of the system, we will make adjustments to ensure the optical system is stable. A test run before experiments will be performed to make sure the drift of optical system is minimized. Based on the principle of thin film interference, the RIM is very sensitive in detecting changes in the thickness of different layers. To investigate the detection sensitivity, a control experiment was performed. In the control experiment, no potential was applied to induce SEI evolution on the substrate, while the optical images of the observation region were kept recording and the recording time was longer than the practical experiment time that containing the entire SEIs evolution process. Thus, the obtained optical signal variation will response to the background noise introduced by system instability or pixel noise. According to statistical analysis (**Supplementary Fig. 14a**), intensity change caused by the background noise is within ±0.5%. Combining the statistical data and the simulation results (**Supplementary Fig. 13**), the thickness change resulting from the background noise can be calculated. From **Supplementary Fig. 14b**, we can find

that for both inner LiF-rich layer and outer organic-rich layer, the noise induced thickness errors are both within 0.3 nm, indicating the high sensitivity of our characterization method.

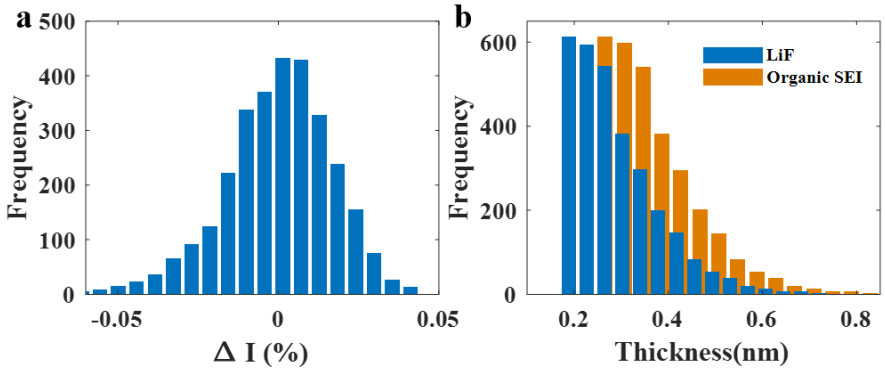

Supplementary Fig. 14 | The detection sensitivity for the inner LiF-rich layer and outer the organic-rich layer. a, The detected intensity change distribution introduced by background and pixel noise. **b,** The calculated theoretical thickness of different layers caused by the background noise.

Section 7. XPS characterization

1. Experiment design.

To understand the entire reaction process, we have measured the composition of SEI layer with XPS at 1.4 V (after the formation of LiF-rich proto-SEI's formation) and 0.1 V (after the organic-rich outer SEI's formation). For each potential, we have measured two samples which were prepared with and without 50 ppm of water as additive in 1 M $LiPF_6$ in propylene carbonate (PC). For certain samples, we also performed the composition profiling at different depths of SEI layer using the XPS with the sputtering function.

2. Experimental procedures

To prepare the sample, we have scanned the potential from 2.3 V to 1.4 and 0.1 V, respectively, and held at the end potential for 100 s so the SEI formation would be completed. After the SEI's formation, the samples were thoroughly cleaned using dimethyl carbonate (DMC), dried in Ar and then directly transferred

from the glove box to the XPS machine without the exposure to any ambient air to prevent the oxidation and the contamination. The measurement was performed in the Pacific Northwest National Laboratory's characterization facility.

3. Measurements and analysis

The XPS measurements were performed with a Thermo Fisher NEXSA with a focused monochromatic Al Kα (1468.7 eV) source for excitation and a doble-focusing hemispherical analyzer. A 300 eV monoatomic Ar+ ions was used for depth profiles sputtering, and the sputter rate was ~ 0.02nm/s calibrated with a known thickness of Ta_2O_5/Ta. Thus, regardless of the SEI composition and porosity, after sputtering 450 s, the estimated removing thickness was ~ 9 nm.

XPS data processing, compositional curve fitting and corresponding area calculation wer performed with CasaXPS software (version 2.3.25) using Gaussian/Lorentz line shapes (50% Gaussian) and the Shirley background correction. All the spectra were calibrated with hydrocarbon C 1s set to 285.0 eV.

4. SEI compounds fitting and analysis

Chemical compositions at different depths of SEI layer were characterized using the XPS. **Supplementary Fig. 15** and **Supplementary Fig. 16** show the chemical compositions after different sputtering times. As the sputtering time increases, the concentration of organic species (ROCOOLi, RCOOLi, etc.) that are labelled with yellow bar in **Supplementary Fig. 15** gradually decreases. Simultaneously, the inorganic species including Li2O and Li2CO3 increase. The characterization results clarify the structural feature of SEI in a more detailed and intuitive method, that the outer SEI layer is enriched by organic chemicals and the inner SEI layer is mainly composed by inorganic species.

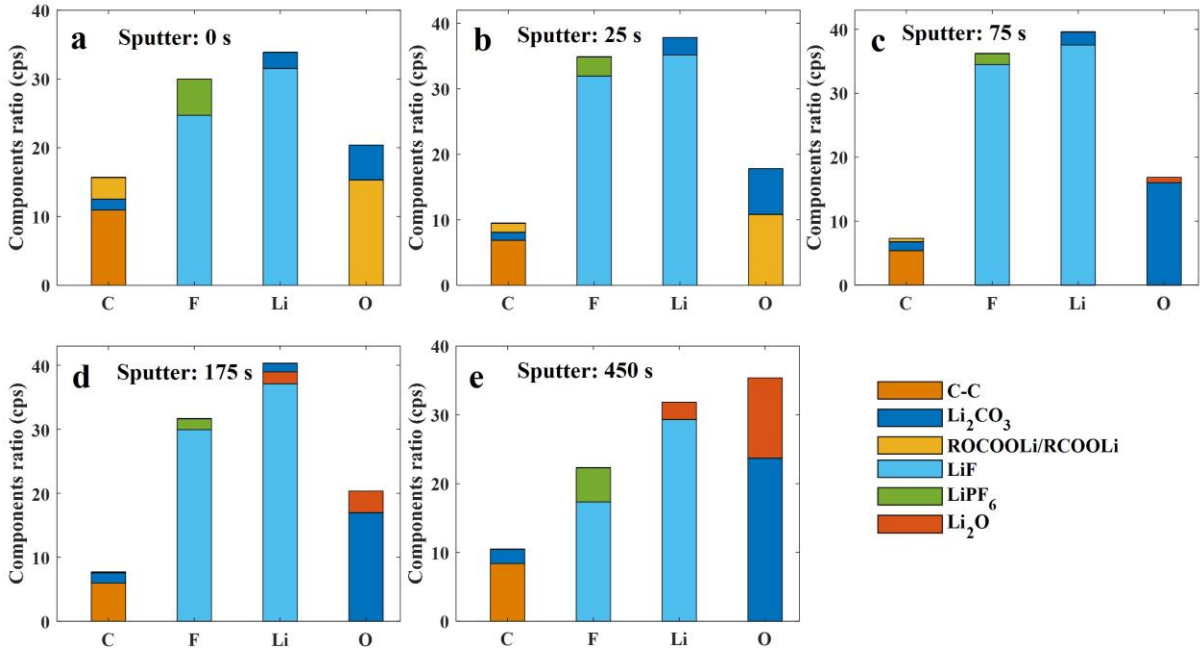

Supplementary Fig. 15 | SEI composition analysis at different depths. (a-e), Relative concentration of SEI compositions formed at different sputtering time of 0 s (corresponded to the **Fig. 3c**), 25 s, 75 s, 175 s, and 450 s (corresponded to the **Fig. 3d**), correspondingly.

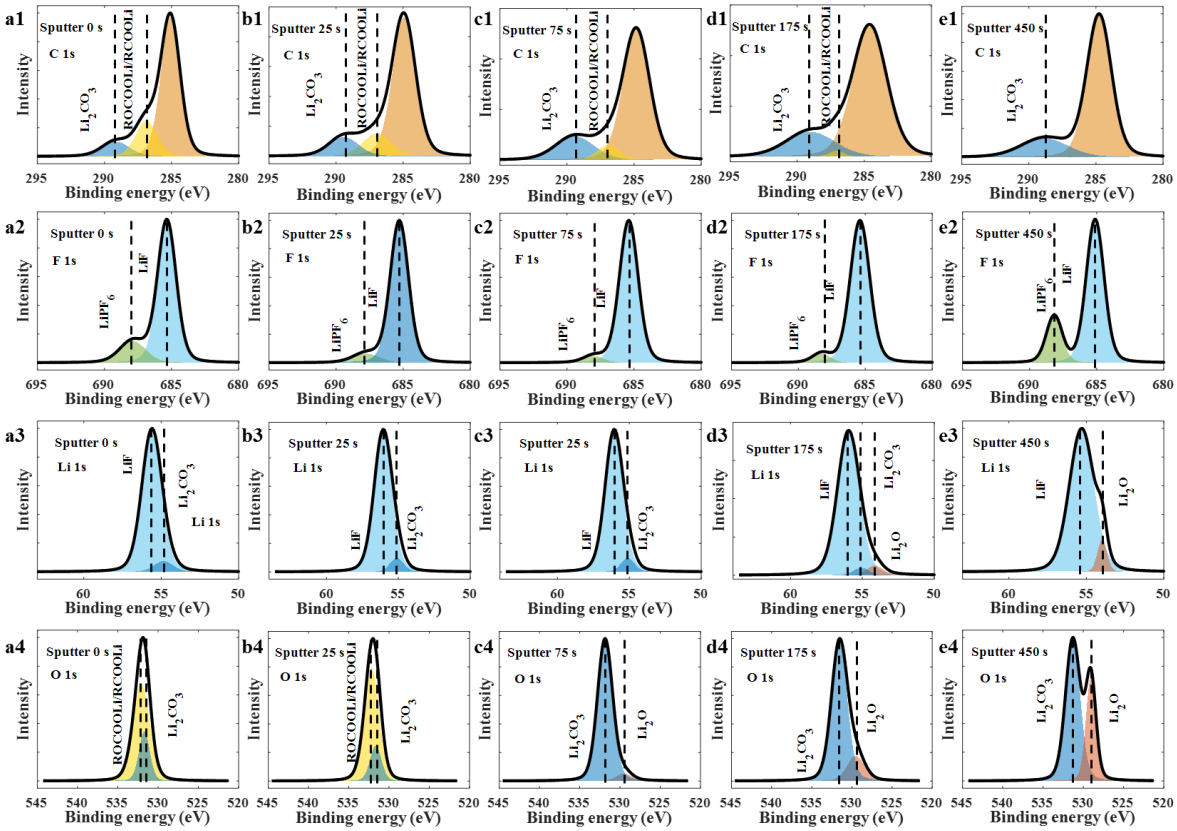

Supplementary Fig. 16 | SEI compounds analysis. (a1-e1), spectra components of C 1s, **(a2-e2)**, spectra components of F 1s, **(a3-e3)**, spectra components of Li 1s, **(a4-e4)**, spectra components of O 1s, at sputtering time of 0 s (corresponded to the **Fig. 3c**), 25 s, 75 s, 175 s, and 450 s (corresponded to the **Fig. 3d**), correspondingly.

Section 8. SEI formation dynamics and galvanostatic deposition

1. SEI formation dynamics.

RIM provides dynamic imaging capability, and we have successfully mapped the localized SEI layers' morphology over time in **Fig.4 (a-f)**. **Supplementary Video 1** and **2** show the LiF-rich and organic-rich SEI layers' morphologies evolution at different potentials. We can see that the pattern of the morphology is gradually formed on the electrode surface, which further proves the surface roughness of SEI is not from the random optical noise, clarifying that RIM allows us to track the SEI layer's growth in different electrolytes and additives and provide a better understanding for electrolyte design. Utilizing the SEI

formation dynamics, the growth rates of LiF-rich SEI layer and organic rich SEI layer can be further calculated and plotted in **Supplementary Fig.17**. The calculated growth rates of both LiF-rich SEI and organic SEI show high consistency with the current density response curve during potential scanning. The results are reasonable since the larger reduction current density response indicates more reactions happen and therefore, we observe higher growth rate of SEI layer. When only a small number of reactions occur, the current density response will be relatively small and correspondingly the growth rate will be slow.

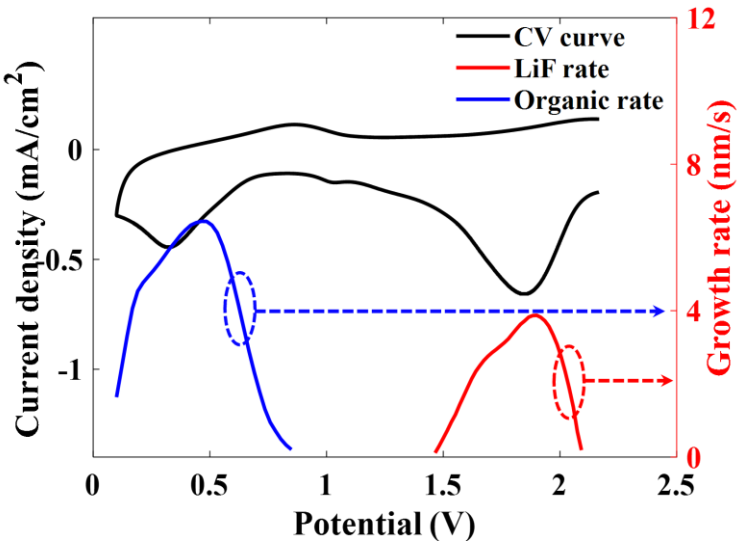

Supplementary Fig. 17 | Growth rate of SEI layers at different potentials. Black curve: CV response of first cycle in 1M $LiPF_6$ in PC with 50 ppm water additive. Blue curve: growth rate of organic-rich SEI layer. Red curve: growth rate of organic-rich SEI layer.

2. Optical and potential response during galvanostatic deposition.

For constant current deposition process, the voltage profiles and optical signals are plotted as a function of time for detailed analysis (**Supplementary Fig. 18**). Almost the same with CV scanning, except for the Li deposition region, the optical signals can be divided into three parts: inner LiF-rich inorganic layer formation, electrical double layer (EDL) accumulation and organic SEI layer deposition. In part I (marked with green in **Supplementary Fig. 18**), from open circuit potential to ~1.3 V, the LiF-rich species are generated after the initial copper oxides reduction leads to increasing optical intensity. Between the potential from 1.3 V to 0.8 V in part II (marked with blue in **Supplementary Fig. 18**), the electrolyte remains thermodynamically stable, and the EDL will form on top of the deposited LiF-rich layer, causing a small drop in the optical signal. And part III (marked with red in **Supplementary Fig. 18**) is located in the left region that above 0 V, where the main electrolyte decomposition happens to produce organic-rich species and results in fast optical signal decreasing. In the control electrolyte, the voltage curve drops quickly from open circuit potential to ~1 V with small optical signal increase. However, in the electrolyte with 50 ppm water additive, two voltage plateaus locate at ~2.8 V and ~2.2 V can be easily observed, both of which could be ascribed to the reduction reactions that formed LiF-rich species[11]. As a result, the optical response is significantly larger, indicating that the inner LiF-rich layer will be considerably thicker than that formed in the control electrolyte.

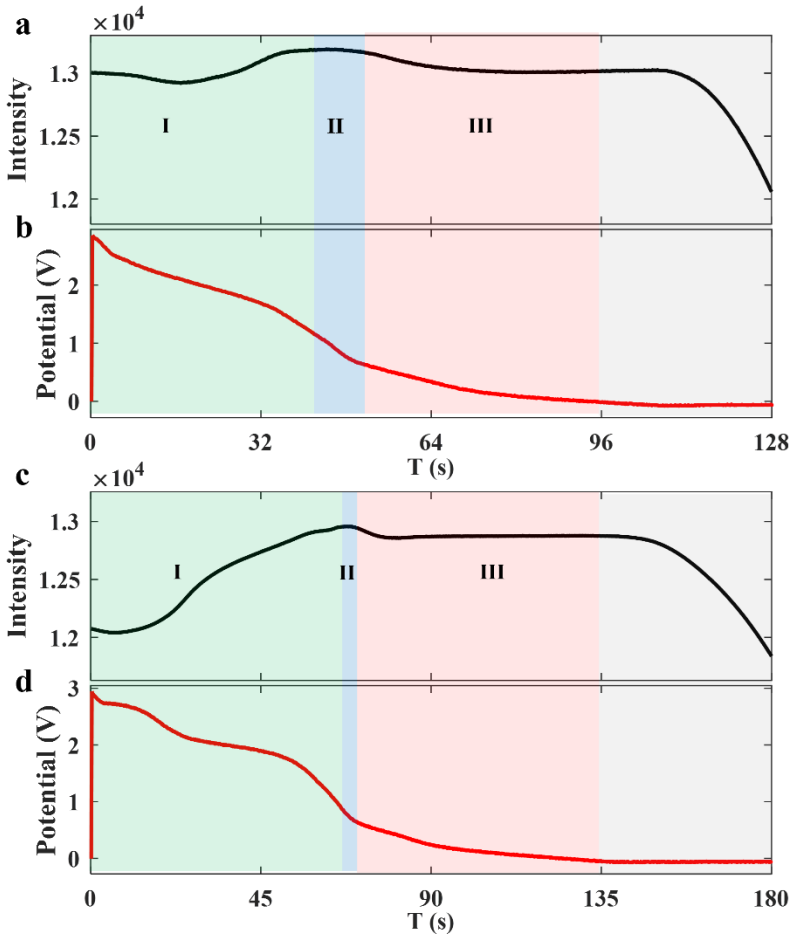

Supplementary Fig. 18 | *In-situ* characterization of the dynamic formation of SEI on Cu surface with constant current density. (a-b) The optical signal and the potential response under the constant current density of 0.1 mA cm^{-1} in control electrolyte. **(c-d)** The optical signal and the potential response under the constant current density of 0.1 mA cm^{-1} in electrolyte with 50 ppm H_2O additive.

3. Li nucleation.

The region below 0 V (black background marked region) is ascribed to Li electroplating process, the newly formed nucleus appears as black spots in our field of imaging (**Supplementary Fig. 19**), and therefore the optical curve would dramatically drop.

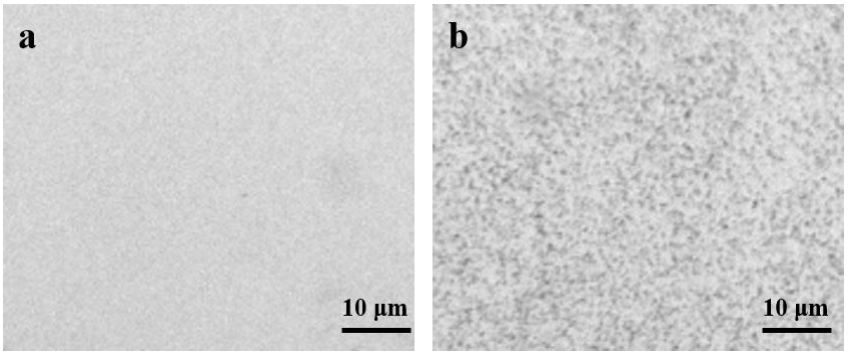

Supplementary Fig. 19 | Nuclei formed on the substrate. a, The substrate surface before Li nucleation happened. **b,** The optical image of the substrate after the nuclei formation.

We have performed the SEM image before and after the Li deposition to show that the Li has successfully deposited on the electrode surface. For the sample with Li, cathodic current density of 0.1 mA cm^{-2} was applied for 200 s to deposit Li on the electrode surface. After deposition, the samples were thoroughly cleaned using dimethyl carbonate (DMC) for three times and dried in Ar. Then the electrode with Li deposition and the clean electrode were loaded in a customized seal box to directly transferred samples from the glove box to the SEM chamber without the exposure to any ambient air to prevent the oxidation and the contamination.

Supplementary Fig. 20a shows the morphology of clean electrode surface and no obvious features are observed. On the other hand, the electrode with Li deposition shown in **Supplementary Fig. 20b** exhibits different behavior. These white particles (pointed by black arrows) in **Supplementary Fig. 20b** result from the Li metal particles that formed during galvanostaic deposition.

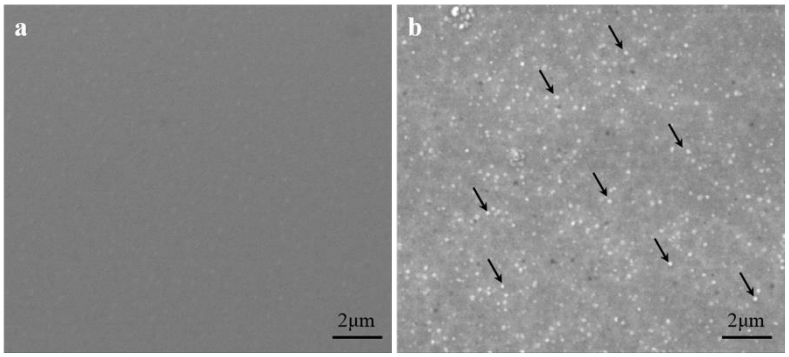

Supplementary Fig. 20 | SEM images. a, Before Li deposition. **b,** After galvanostatic deposition of 200 s.

4. Thickness of SEI layers formed in galvanostatic deposition

The thicknesses of LiF-rich layers in the constant current experiments are much thicker than their counterparts formed under potentiodynamic polarization tests. Taking the water containing electrolyte as an example, the constant current experiment generates a ~ 63 nm thick LiF-rich layer while the thickness of LiF-rich layer in CV scan experiment is only ~23 nm (**Fig. 2b**). This is because when applied cyclic voltammetry (CV), due to the fast scan rate the reaction capacity is relatively small because the HF near the electrode interface would deplete very quickly, which leads to less LiF accumulation. However, when a small constant current of 0.1 mA/cm^2 was applied, more HF would diffuse to the interface, increasing the reaction capacity and therefore more HF would be reduced to form LiF. Through calculations, it turned out that the total charge consumed to generate the LiF-rich layer under galvanostatic condition is larger than the potentiodynamic polarization tests, which also indicated that more LiF-rich layer was produced. As expected, the organic-rich layer thickness is merely ~ 8 nm in this case, much thinner than that obtained by CV scans (~ 30 nm). Similar to results obtained from CV scans, the presence of 50 ppm water leads to a thicker LiF-rich layer (63 nm vs 22 nm). This again verifies that the effect of water additive on the formation of LiF layer, regardless of the electrochemical condition that forms it.

Section 9. Electrochemical impedance spectroscopy measurement

1. Sample preparation and experimental procedure

The electrodes were prepared by scanning the potential from 2.4 V to 1.4 V (Sample #1), 1.0 V (Sample #2) and 0.1 V (Sample #3), respectively. The impedance tests were performed when the working electrodes were held at the same potentials. The voltage amplitude was 5 mV and frequency varied from 100 kHz to 0.1 Hz.

2. Impedance data analysis

Supplementary Fig. 21 shows the impedance spectra obtained on these three samples. In Sample #1 and #2, the SEI layers were formed by scanning potential from 2.4 to 1.4 V and 1.0 V, respectively. Therefore, the dominant SEI layer on the electrode surface is the LiF-rich layer. Both spectra consist of a semicircle and a sloping line. The semicircle observed at high frequency is correlated to the LiF-rich layer formed on the electrode, and the sloping line at low frequency corresponds to the ions that are accumulated on the electrode. For sample #3, since the electrode was scanned from 2.4 V to 0.1 V, both LiF-rich and organic SEI layers are both presented on the surface. Therefore, we can clearly see two different semicircles in the fitting results.

We have also compared the resistance and the capacitance numbers that are fitted from the impedance curves. The fitting parameters were summarized in **Supplementary Table 2** and the overall resistance and capacitance of the SEI can be calculated by the following equations:

$$R_{SEI} = R_{SEI1} + R_{SEI2}$$

$$\frac{1}{C_{SEI}} = \frac{1}{C_{SEI1}} + \frac{1}{C_{SEI2}}$$

The resistances of SEI layer, which is corresponded to the leakage current, were 5138 Ω, 6950 Ω, and 9410 Ω (total resistance from R_{SEI1} + R_{SEI2}) for Sample #1, #2, and #3, respectively. The R_{SEI} of Sample #1 is a little smaller than that of Sample #2, which is due to the thicker LiF-rich layer deposited on the electrode

surface. When we further scan the electrode down to 0.1 V, the organic SEI layer starts to form on top of the LiF-rich layer. This will significantly increase the resistance. The total SEI resistance (R_{SEI1} + R_{SEI2}) of Sample #3 is almost two times of the Sample #1, which proves the deposition of the organic layer will provide better insulation. At the same time, the capacitance of Sample #3 decreases compared with Sample #1 and #2, which is due to the increase of the SEI layer's thickness caused by the organic SEI's deposition. This is additional evidence which can prove the deposition of organic SEI layer.

Supplementary Table 2

Potential (V)	R_{SEI1} (Ω)	CPE_1 (μF)	R_{SEI2} (Ω)	CPE_2 (μF)	CPE_{Acc}(μF)
1.4	5138	2.06			7.55
1.0	6950	1.52			8.72
0.1	4079	1.07	5330	1.64	17.39

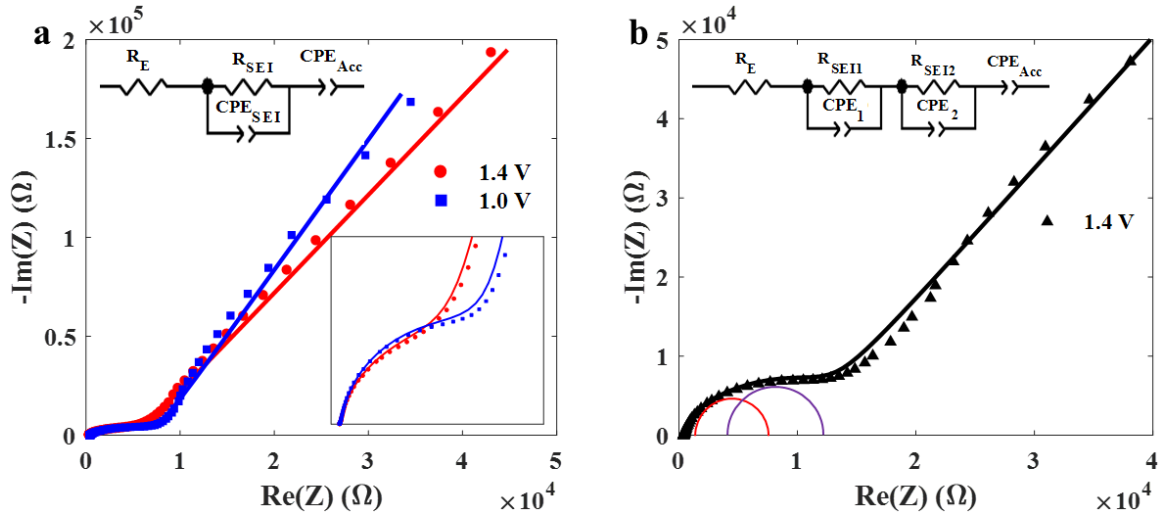

Supplementary Fig. 21 | Impedance analysis of the electrodes with different SEI layers. a, Impedance spectra and their fitting curves on the surface that the LiF-rich layer is dominated. **b,** Impedance spectrum and the fitted curves on the electrode that has both LiF-rich and organic SEI layers.

References

1. Aurbach D, Daroux M, Faguy P, Yeager EJJoTES. Identification of surface films formed on lithium in propylene carbonate solutions. 1987, **134**(7)**:** 1611.

2. Zhuang GV, Xu K, Yang H, Jow TR, Ross PNJTJoPCB. Lithium ethylene dicarbonate identified as the primary product of chemical and electrochemical reduction of EC in 1.2 M LiPF6/EC: EMC electrolyte. 2005, **109**(37)**:** 17567-17573.

3. Xu KJCr. Nonaqueous liquid electrolytes for lithium-based rechargeable batteries. 2004, **104**(10)**:** 4303-4418.

4. Mozhzhukhina N, Flores E, Lundström R, Nyström V, Kitz PG, Edström K*, et al.* Direct operando observation of double layer charging and early solid electrolyte interphase formation in Li-ion battery electrolytes. 2020, **11**(10)**:** 4119-4123.

5. Shadike Z, Lee H, Borodin O, Cao X, Fan X, Wang X*, et al.* Identification of LiH and nanocrystalline LiF in the solid–electrolyte interphase of lithium metal anodes. 2021, **16**(5)**:** 549-554.

6. Jin Y, Zhou L, Yu J, Liang J, Cai W, Zhang H*, et al.* In operando plasmonic monitoring of electrochemical evolution of lithium metal. 2018, **115**(44)**:** 11168-11173.

7. Kitta M, Murai K, Yoshii K, Sano HJJotACS. Electrochemical Surface Plasmon Resonance Spectroscopy for Investigation of the Initial Process of Lithium Metal Deposition. 2021, **143**(29)**:** 11160-11170.

8. Shi Y, Feng G, Li X, Yang X, Ghanim AH, Ruchhoeft P*, et al.* Electrochemical Impedance Imaging on Conductive Surfaces. *Anal Chem* 2021, **93**(36)**:** 12320-12328.

9. Haltom T, Arakawa E, Williams M, Kretschmann EJAo. Refractive index of LiF films as a function of time. 1979, **18**(8)**:** 1233-1236.

10. Al-Kuhaili MJJoVS, Technology A: Vacuum S, Films. Chemical and optical properties of thermally evaporated manganese oxide thin films. 2006, **24**(5)**:** 1746-1750.

11. Qian J, Xu W, Bhattacharya P, Engelhard M, Henderson WA, Zhang Y*, et al.* Dendrite-free Li deposition using trace-amounts of water as an electrolyte additive. 2015, **15:** 135-144.